











RESEARCH ARTICLE | JANUARY 31 2024

Reversible solvent interactions with UiO-67 metal–organic frameworks

Special Collection: [Porous Solids for Energy Applications](#)

Isabella Goodenough ; Mikaela C. Boyanich ; Ryan P. McDonnell ; Lauren Castellana ;
Venkata Swaroopa Datta Devulapalli ; Tian-Yi Luo ; Prasenjit Das ; Mélissandre Richard ;
Nathaniel L. Rosi ; Eric Borguet 



J. Chem. Phys. 160, 044711 (2024)

<https://doi.org/10.1063/5.0180924>



CrossMark



The Journal of Chemical Physics

Special Topic: Algorithms and Software for Open Quantum System Dynamics

Submit Today

Reversible solvent interactions with UiO-67 metal-organic frameworks

Cite as: J. Chem. Phys. 160, 044711 (2024); doi: 10.1063/5.0180924

Submitted: 12 October 2023 • Accepted: 6 December 2023 •

Published Online: 31 January 2024













View Online



Export Citation



CrossMark

Isabella Goodenough,¹  Mikaela C. Boyanich,^{1,a)}  Ryan P. McDonnell,^{1,b)}  Lauren Castellana,¹ 
Venkata Swaroopa Datta Devulapalli,¹  Tian-Yi Luo,²  Prasenjit Das,²  Mélissandre Richard,^{1,c)} 
Nathaniel L. Rosi,²  and Eric Borguet^{1,d)} 

AFFILIATIONS

¹ Department of Chemistry, Temple University, Philadelphia, Pennsylvania 19122, USA

² Department of Chemistry, University of Pittsburgh, Pittsburgh, Pennsylvania 15261, USA

Note: This paper is part of the JCP Special Topic on Porous Solids for Energy Applications.

a) Present address: Department of Chemistry, Virginia Tech, Blacksburg, Virginia 24601, USA.

b) Present address: Department of Chemistry, University of Wisconsin – Madison, Madison, Wisconsin 53706, USA.

c) Present address: Univ. Lille, CNRS, Centrale Lille, Univ. Artois, UMR 8181, UCCS - Unité de Catalyse et Chimie du Solide, 59000 Lille, France.

d) Author to whom correspondence should be addressed: eborguet@temple.edu

ABSTRACT

The utility of UiO-67 Metal-Organic Frameworks (MOFs) for practical applications requires a comprehensive understanding of intermolecular host-guest MOF-analyte interactions. To investigate intermolecular interactions between UiO-67 MOFs and complex molecules, it is useful to evaluate the interactions with simple polar and non-polar analytes. This problem is approached by investigating the interactions of polar (acetone and isopropanol) and non-polar (n-heptane) molecules with functionalized UiO-67 MOFs via temperature programmed desorption mass spectrometry and temperature programmed Fourier transform infrared spectroscopy. We find that isopropanol, acetone, and n-heptane bind reversibly and non-destructively to UiO-67 MOFs, where MOF and analyte functionality influence relative binding strengths (n-heptane \approx isopropanol $>$ acetone). During heating, all three analytes diffuse into the internal pore environment and directly interact with the μ_3 -OH groups located within the tetrahedral pores, evidenced by the IR response of $\nu(\mu_3\text{-OH})$. We observe nonlinear changes in the infrared cross sections of the $\nu(\text{CH})$ modes of acetone, isopropanol, and n-heptane following diffusion into UiO-67. Similarly, acetone's $\nu(\text{C=O})$ infrared cross section increases dramatically when diffused into UiO-67. Ultimately, this *in situ* investigation provides insights into how individual molecular functional groups interact with UiO MOFs and enables a foundation where MOF interactions with complex molecular systems can be evaluated.

Published under an exclusive license by AIP Publishing. <https://doi.org/10.1063/5.0180924>

INTRODUCTION

Unavoidable consequences of large-scale chemical production are the generation of harmful byproducts and emission of volatile organic compounds (VOCs).¹ Such anthropogenic pollutants are known to have damaging effects on humans and environmental health, including depletion of the ozone layer and production of photochemical smog, which has warranted stricter environmental guidelines and remediation strategies.^{2–4} Adsorptive removal of hazardous chemical species is an effective decontamination strategy, given the low cost, lack of chemical degradation, and ease of sorbent regeneration.² The effectiveness of a sorbent material

relies on a combination of its high adsorption capacity, analyte selectivity, durability, ease of regeneration, and stability.^{2,4,5} The current industrial standard involves the use of carbonaceous materials (e.g., activated carbon materials),⁶ which are limited by inherent challenges, such as chemical saturation and the potential for insufficient filtration and, thus, re-emission back into the environment.⁷

Zirconium-based Metal-Organic Frameworks (MOFs), and especially the UiO-67 series of MOFs, are particularly well suited as superior sorbent materials.^{8–11} MOFs are hybrid structures, consisting of inorganic metal or metal-oxide nodes and organic bridging linkers, which offer unique, tunable properties, which

can be optimized for the capture and storage of industrial chemicals.⁷ The ease of framework modulation separates MOFs from traditional organic or inorganic porous materials, which are often limited by a lack of structural and chemical diversity, rendering them impractical for targeted applications.^{4,5,12,13} Of particular interest, UiO-67 Zr-based MOFs, built from $Zr_6O_4(OH)_4(COO)_{12}$ secondary building units (SBUs) linked with polytopic linear carboxylate ligands, are known for their physiochemical and thermal stabilities.^{5,14,15} UiO-67 series MOFs have demonstrated resilience toward a variety of chemical environments and thus offer inherent advantages for filtration (via sorption)-based applications over other MOFs.^{4,13,16}

Developing an understanding of the characteristic binding interactions of simple polar and non-polar solvents with UiO-67-X MOFs provides insights into the fundamental behavior of Zr-MOFs and a basis for which more complicated molecular systems can be investigated. Using a combination of temperature-programmed desorption mass spectrometry (TPD-MS) and *in situ* temperature-programmed infrared (TP-IR) spectroscopy to identify solvent adsorption sites, we investigate the binding of three simple solvents: acetone, isopropanol, and n-heptane with UiO-67 and the functional analogs UiO-67-NH₂ and UiO-67-CH₃. We find that the studied solvents bind reversibly to UiO-67-X MOFs. Comparing the binding energies of the three solvents with UiO-67 reveals a quantitative trend in binding strength: n-heptane \approx isopropanol > acetone, which suggests that analyte and MOF functionality is more important than polarity in predicting MOF-analyte binding interactions. The interactions of UiO-67 with the polar analytes, acetone and isopropanol, are dominated by hydrogen bonding, evident by the evolution of unique OH signals that evolve as the analytes diffuse into the MOF pores during heating. The binding of the non-polar analyte, n-heptane, with the MOF likely results from a combination of dispersion interactions with the organic linker and weak interactions with the μ_3 -OH groups,¹⁷ perturbing the local environment around the inorganic SBU. *In situ* investigation of temperature-dependent MOF-guest interactions provides insights into how individual functional groups interact with UiO MOFs, enabling a foundation where MOF-molecule interactions can be evaluated.

EXPERIMENTAL

MOF synthesis and characterization

UiO-67-X (X: H, NH₂, and CH₃) were synthesized as described previously.¹⁸ Relevant powder x-ray diffraction (PXRD) patterns can be found elsewhere.^{18–20}

Temperature programmed studies

Temperature programmed desorption mass spectrometry (TPD-MS) and temperature programmed Fourier transform infrared (TP-IR) spectroscopy experiments were conducted under ultra-high vacuum (UHV; $p < 1.0 \times 10^{-8}$ Torr after bakeout) using custom-built stainless steel UHV instruments described in detail previously.^{21,22} MOF samples were pasted onto a tungsten grid (Alfa-Aesar, 25 μ m thickness), which was braced to a copper sample holder fixed to a manipulator. A fast-response K-type thermocouple

(Omega, 0.002 in. diameter) was directly spot-welded to the grid adjacent to the MOF to monitor sample temperature. This arrangement allowed for rapid sample cooling to cryogenic temperatures (~ 100 K) and resistive heating using direct current from a power supply (Model no. SCR 10-80, Electronic Measurements Inc.).

Infrared spectra were recorded in real time via a FT-IR spectrometer (Bruker, Tensor 27) in a transmissive geometry between 4000 and 400 cm^{-1} at 4 cm^{-1} resolution with a room temperature DLaTGS detector, averaged over 16 scans (6 mm aperture, 10 kHz scanning velocity). A 64-scan background of the W mesh at room temperature (~ 295 K) was recorded and applied to all collected spectra. TP-IR spectra are presented as difference spectra, $\Delta I(\tilde{\nu}, T) = I(\tilde{\nu}, T) - I_0(\tilde{\nu}, T)$, where an infrared spectrum of the clean MOF at some temperature T , I_0 , is subtracted from an infrared spectrum of the MOF and analyte, I , at roughly the same temperature T . $\tilde{\nu}$ is a wavenumber (units of cm^{-1}). This procedure is performed due to heating effects present in the infrared spectra of UiO-67-X.²³ It is known that the infrared absorbance of porous materials can change due to optical scattering.²⁴ Since baseline correction appears to quantitatively restore IR absorption values in the 1600–4000 cm^{-1} region (Figs. S6–S8), scattering contributions in the analysis of integrated infrared absorbance are neglected.

MOF samples suspended in dimethylformamide (DMF) were centrifuged at 14 000 rpm for 5 min. After centrifugation, the supernatant solvent was removed, whereby the resulting MOF pellet (typically ~ 2 mg) was uniformly pasted as a pinhole free disk (6–8 mm in diameter, 25–50 μ m thick) onto a clean tungsten grid (Alfa-Aesar) and introduced into the UHV chamber. The resulting optical density measured by IR was on the order of 0.5–1.0. Baking the chamber at ~ 373 K for 18–24 h removed residual atmospheric gases (e.g., N₂, CO₂, and water vapor) and laboratory contaminants (e.g., volatile organics) adhered onto the sample and chamber walls.

After bakeout, UiO-67 and UiO-67-NH₂ samples were activated for 1 h at 473 K, while UiO-67-CH₃ samples were activated for 1 h at 423 K.¹⁸ Complete removal of the confined solvent (DMF) and residual water was confirmed using IR spectroscopy through the lack of infrared absorbance in the 3400 cm^{-1} region following thermal activation (Fig. S1).

Desired analyte exposures were achieved by backfilling the UHV chamber at constant pressure (1.0×10^{-5} Torr), monitored with a nude ion gauge (Duniway iridium filament) over a fixed time interval. Exposures, measured in langmuirs, L ($1 \text{ L} \equiv 10^{-6}$ Torr-s), are calculated via uncorrected ion gauge measurements (Granville Phillips 307). The approximate exposure for all experiments is ~ 1100 L. After dosing, the leak valve is closed and the pressure inside the chamber drops as the system is pumped down to the desired pressure ($< 1.0 \times 10^{-8}$ Torr) before the temperature ramp is initiated.

Following analyte exposure (while the sample was held at 100 K) the sample temperature was ramped at 2.0 K/s (TPD-MS) or 1.0 K/s (TP-IR) to the activation temperature (e.g., 473 K). During TPD-MS experiments, the most abundant mass fragments of each solvent were monitored as a function of temperature ($m/z = 43, 45$, and 43 for acetone, isopropanol, and n-heptane, respectively). The analytes acetone (99.5%, ACS Grade, Thermo Fisher Scientific), isopropanol (99.5%, ACS Grade, Thermo Fisher Scientific), and n-heptane (99%, Alfa-Aesar) were purified via

consecutive freeze–thaw cycles. Purity was confirmed using a quadrupole Residual Gas Analyzer (RGA) mass spectrometer (AccuQuad RGA 300, Stanford Research Systems) (Fig. S2). Custom LabVIEW programs (with commercial drivers) were used for both TPD-MS and TP-IR experiments to control the heating process in addition to monitoring temperature and pressure.

Evaluation of analyte binding preferences and energetics through TPD-MS

TPD-MS provides insights into analyte binding, specifically the availability of binding sites and MOF–analyte binding energies. Desorption activation energies, E_{des} , are often calculated via the Redhead equation [Eq. (1)], which assumes first-order desorption, as well as the validity of the Polanyi–Wigner equation, and extracts desorption energies from the temperature at maximum desorption, T_m , as described elsewhere:^{25–27}

$$E_{des}(T_m) = RT_m \left(\ln \left(\frac{\nu T_m}{\beta} \right) - 3.46 \right). \quad (1)$$

In Eq. (1), R , ν , and β are the ideal gas constant, pre-exponential factor (*vide infra*), and heating rate ($\sim 2 \text{ K s}^{-1}$), respectively.

The typical pre-exponential factor for first-order desorption (10^{13} s^{-1}) is unsuitable for describing the desorption of many molecules.^{21,28–31} To account for the dependence of the pre-exponential factor on molecular properties and desorption temperature, we write ν , in the low coverage limit, through transition state theory as

$$\nu(T_m) = \frac{k_B T_m}{h} \frac{q^\ddagger(T_m)}{q(T_m)}, \quad (2)$$

where k_B is the Boltzmann constant, h is Planck's constant, q^\ddagger is the transition state partition function, and q is the adsorbate partition function.^{31,32} Note that here, ν is taken to be coverage independent. We presume that the partition function of the adsorbed molecule (q) is unity. This approximation assumes that low frequency translations, rotations, and vibrations do not significantly contribute to the adsorbate partition function. This approach has satisfactorily described the pre-exponential factors of small, polar species and large, non-polar species.^{29–31} Conversely, it is taken that the dominating contributions of the transition state partition function, q^\ddagger , are the rotational and translational degrees of freedom.³¹ We thus approximate (2) as

$$\nu(T_m) \approx \frac{k_B T_m}{h} q_r^\ddagger(T_m) q_t^\ddagger(T_m), \quad (3)$$

where q_r^\ddagger (q_t^\ddagger) is the 3D rotational (2D translational) partition function.³¹ In the high temperature limit,³³ q_r^\ddagger for a 3D asymmetrical top in the rigid rotor approximation is written as

$$q_r^\ddagger(T_m) = \frac{1}{\sigma} \left(\frac{k_B T_m}{hc} \right)^{3/2} \left(\frac{\pi}{\tilde{A} \tilde{B} \tilde{C}} \right)^{1/2}, \quad (4)$$

and q_t^\ddagger , assuming a 2D gas,^{29,34} is written as

$$q_t^\ddagger(T_m) = A \cdot \left(\frac{h}{\sqrt{2\pi m k_B T_m}} \right)^{-2} = A \frac{2\pi m k_B T_m}{h^2}, \quad (5)$$

where σ is a symmetry number, c is the speed of light (in cm s^{-1}), \tilde{A} , \tilde{B} , \tilde{C} are the rotational spectroscopic constants (in cm^{-1}), A is the molecular surface area (in m^2), and m is the analyte mass (in kg).³³ This yields a final expression of

$$\begin{aligned} \nu(T_m) &= \frac{1}{\sigma} \frac{k_B T_m}{h} \left(\frac{k_B T_m}{hc} \right)^{3/2} \left(\frac{\pi}{\tilde{A} \tilde{B} \tilde{C}} \right)^{1/2} \left(A \frac{2\pi m k_B T_m}{h^2} \right) \\ &= \nu_0 T_m^{7/2}. \end{aligned} \quad (6)$$

The \tilde{A} , \tilde{B} , \tilde{C} values are obtained through microwave rotational spectroscopy or computational methods (diagonalizing the ground state geometry inertia tensor).^{35,36} Using values reported elsewhere,^{29,37,38} we calculate approximate pre-exponential factors for all three analytes considered in this study (Table I). We consider rotational constants for the gauche conformation of isopropanol as it has been observed to be more stable.^{38,39} Based on previous studies, we take $A = 10^{-19} \text{ m}^2$, the reciprocal of the average surface density (10^{19} m^{-2}).³¹ From these values and Eqs. (1) and (6), we evaluate E_{des} through^{25,40}

$$E_{des}(T_m) = RT_m \left(\ln \left(\frac{\nu_0 T_m^{7/2}}{\beta} \right) - 3.46 \right). \quad (7)$$

TPD-MS experiments were carried out on the selected analytes by monitoring the most abundant molecular ion fragments ($m/z = 43, 45, \text{ and } 43$ for acetone, isopropanol, and n-heptane, respectively) as the MOF samples were heated under UHV following analyte exposure. Since the TPD-MS profiles of all major analyte mass fragments show identical behavior modulo scaling factors (Figs. S3–S5), the analytes appear to molecularly physisorb to UiO-67-X.⁴¹

In this study, we investigate the binding interactions at low analyte coverage ($< 10\%$ of a complete monolayer) to minimize adsorbate–adsorbate interactions and enable the unique identification of MOF–analyte interactions within the internal pore environment. We estimate that an $\sim 1100 \text{ L}$ analyte dose corresponds to $\sim 2\%$ of the total available MOF surface area. See the supplementary material for more details.

TABLE I. Parameters used to generate pre-exponential factors.^{29,37,38} Where possible, rotational constants are truncated with order 10^{-5} . For isopropanol, we consider rotational constants for its symmetric, gauche form.

Quantity	Acetone ³⁷	Isopropanol ³⁸	n-heptane ²⁹
σ	2	1	2
\tilde{A} (cm^{-1})	0.339 08	0.288 17	1.232
\tilde{B} (cm^{-1})	0.284 03	0.269 03	0.079
\tilde{C} (cm^{-1})	0.163 79	0.159 10	0.076
m (kg)	9.6346×10^{-26}	9.9667×10^{-26}	1.6611×10^{-25}
ν_0 ($\text{K}^{-7/2} \text{ s}^{-1}$)	1.626×10^{11}	3.806×10^{11}	4.101×10^{11}

RESULTS AND DISCUSSION

Acetone binding in UiO-67-X MOFs

The quantity and position of peaks in the TPD-MS spectrum provide information on the availability and strength of available analyte binding sites on UiO-67-X MOFs. Following acetone exposure, TPD-MS spectra are generated by monitoring the $m/z = 43$ molecular ion fragment as UiO-67-X samples are heated under UHV from 100 to 473 K at ~ 2.0 K s^{-1} [Fig. 1(a)]. Acetone desorption occurs in two temperature regions: a low temperature region around 150 K and a high temperature region between 180–260 K [Fig. 1(a)]. The asymmetric line shape and common leading edge observed for the low temperature feature near 150 K, similar to previous studies of acetone desorption from carbonaceous materials,^{21,41,42} are consistent with a zero-order process that likely originates from desorption of a condensed acetone multilayer.^{43,44}

As the sample temperature increases, some acetone molecules desorb from the condensed multilayer on the external crystallite surfaces ($T_m \sim 150$ K, site 1), while the remaining acetone molecules diffuse into and bind to sites within the internal pore environment from which they subsequently desorb ($T_m > 150$ K). For UiO-67-CH₃, we observe a larger contribution from the low temperature site compared to UiO-67 and UiO-67-NH₂ [Fig. 1(a)]. It appears that more acetone molecules remain on the external UiO-67-CH₃ surface, likely due to repulsive interactions induced by the methyl substituent.

Acetone binding in UiO-67-X MOFs is assessed through the modified Redhead equation [Eq. (7)]. We note that two higher energy desorption sites ($T_m > 150$ K) are observed for UiO-67 with energies of 67.4 kJ/mol ($T_m = 180$ K, site 2) and 86.1 kJ/mol ($T_m = 225$ K, site 3), which indicates that multiple binding sites are accessible within the UiO-67 internal pores at low coverage (Table II). We note that the TPD-MS trace for UiO-67-NH₂ appears to have a line shape change at ~ 263 K, which we suspect is indicative of a higher energy binding site. The trend observed experimentally is UiO-67-NH₂ (102.2 kJ/mol) > UiO-67-CH₃ (90.3 kJ/mol)

TABLE II. Acetone desorption energies calculated through Eq. (7) and values in Table I, assuming a first-order desorption process.

	Site 2		Site 3	
	T_m (K)	E_{des} (kJ/mol)	T_m (K)	E_{des} (kJ/mol)
UiO-67	180	67.4	225	86.1
UiO-67-NH ₂	215	81.9	263	102.2
UiO-67-CH ₃	235	90.3

> UiO-67 (86.1 kJ/mol). It is possible that in UiO-67-CH₃, the acetone molecules that do diffuse into the internal pore environment would preferentially bind within the more polar tetrahedral UiO-67 cavity where the majority of the μ_3 -OH groups on the inorganic SBU reside. Short-range interactions between acetone and the UiO-67-CH₃ methyl substituent may account for this binding energy discrepancy. For UiO-67-NH₂, it is possible that there are competing binding interactions with the amine and μ_3 -OH groups. In order to access the μ_3 -OH groups, the molecule must first pass through the larger pore opening containing the linker amine groups, which likely accounts for majority of the acetone binding interactions at low exposure.

Isopropanol binding in UiO-67-X MOFs

To determine if molecular polarity influences binding properties, isopropanol adsorption on UiO-67-X MOFs was investigated. Isopropanol TPD-MS spectra are created by monitoring the evolution of the $m/z = 45$ mass fragment as the UiO-67-X sample is heated following 1100 L isopropanol exposure. The TPD-MS profiles of UiO-67-X following ~ 1100 L isopropanol exposure reveal several features consistent with multiple adsorption sites at low coverage [Fig. 1(b)]. As the sample temperature is increased, some molecules desorb from the condensed layer ($T_m \sim 174$ K, site 1); the asymmetric line shape and common leading edge for this peak

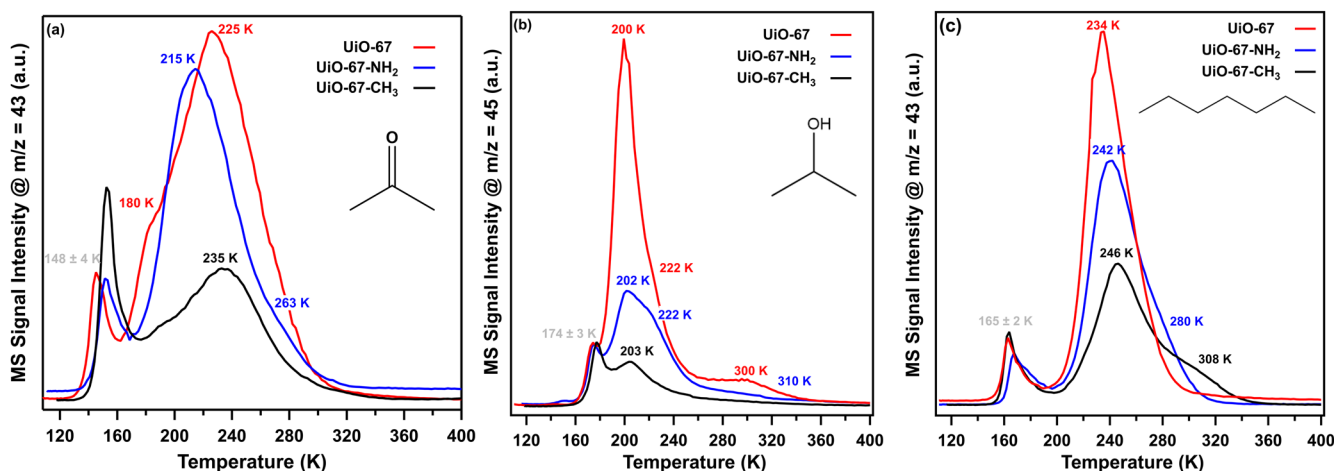


FIG. 1. TPD-MS spectra following ~ 1100 L exposure of analytes, tracking the molecular ion fragments of (a) acetone ($m/z = 43$), (b) isopropanol ($m/z = 45$), and (c) n-heptane ($m/z = 43$) of UiO-67 (red), UiO-67-CH₃ (teal), and UiO-67-NH₂ (blue) during heating from ~ 100 K to T_{act} at ~ 2.0 K/s. The actual dose was within 10% of the target exposure (1100 L) for all UiO-67-X MOFs.

TABLE III. Isopropanol desorption energies calculated through Eq. (7) and values in Table I, assuming a first-order desorption process.

	Site 2		Site 3		Site 4	
	T _m (K)	E _{des} (kJ/mol)	T _m (K)	E _{des} (kJ/mol)	T _m (K)	E _{des} (kJ/mol)
UiO-67	200	77.1	222	86.4	300	120.2
UiO-67-NH ₂	202	77.9	222	86.4	310	124.6
UiO-67-CH ₃	203	78.3

are consistent with a zero-order process at temperatures consistent with reported isopropanol sublimation from carbonaceous and water ice surfaces.^{45–47} Meanwhile, the remaining molecules diffuse into and preferentially bind to the most accessible sites within the MOF pores.⁴⁸ This internal pore binding is identified in the TPD-MS spectra by a common feature near 200 K for all UiO-67-X MOFs [Fig. 1(b)]. Calculated experimental desorption energies yield values of 75.9 kJ/mol (UiO-67), 76.8 kJ/mol (UiO-67-NH₂), and 77.2 kJ/mol (UiO-67-CH₃) (site 2, Table III). The similarity in these energy values strongly suggests that isopropanol is desorbing from the same site in each UiO-67-X MOFs, likely originating from interacting with the inorganic SBU.⁴⁹ For UiO-67 and UiO-67-NH₂, an additional higher temperature desorption peak is observed at 300 K (118.4 kJ/mol, site 3) and 310 K (122.8 kJ/mol), respectively (Table III).

Molecular polarity and MOF functionalization should drive the relative analyte binding strength to UiO-67-X. Isopropanol interactions with UiO-67 and UiO-67-NH₂ are significantly stronger than interactions with acetone (see Table II). We hypothesize this may be related to the ability of isopropanol to act as both a hydrogen bond donor and acceptor, which can enable multiple binding configurations with the MOFs. We note that the TPD-MS trace for isopropanol desorption from UiO-67-CH₃ [Fig. 1(b)] is flat for T > 220 K. We suspect that the flat TPD-MS profile results from short-range interactions with the CH₃ group, weaker than those with the amine functionalized MOF.

n-heptane binding in UiO-67-X MOFs

To complete the analysis, the desorption kinetics of a non-polar, non-protic solvent, n-heptane, from UiO-67-X were investigated. UiO-67-CH₃ appears to have the strongest interactions with the non-polar analyte, n-heptane, as revealed by two higher temperature desorption features at 246 K (96.7 kJ/mol) and 308 K (123.9 kJ/mol) [Fig. 1(c), site 2]. The lower temperature feature observed for UiO-67-CH₃ (246 K) coincides with similar features observed for UiO-67 and UiO-67-NH₂ at 234 K (91.7 kJ/mol) and 242 K (95.1 kJ/mol), respectively, which suggests that n-heptane likely desorbs from a similar site for all UiO-67-X MOFs. Notably, the high temperature shoulder (T_{des} > 250 K) is only observed for the functionalized UiO-67 MOFs [Fig. 1(c), site 3], which suggests that this n-heptane-MOF binding interaction likely originates from interaction with the functional group on the organic linker. The highest temperature n-heptane binding feature (T_m = 308 K) on UiO-67-CH₃ yields the strongest binding energy compared to all other MOF-analyte systems reported here (Table IV). We suspect that this strong binding results from a combination

TABLE IV. n-heptane desorption energies calculated through Eq. (7) and values in Table I, assuming a first-order desorption process.

	Site 2		Site 3	
	T _m (K)	E _{des} (kJ/mol)	T _m (K)	E _{des} (kJ/mol)
UiO-67	234	91.7
UiO-67-NH ₂	242	95.1	286	114.2
UiO-67-CH ₃	246	96.7	308	123.9

of attractive interactions originating from non-polar character of the organic linker (-CH₃ substituent), i.e., dispersion interactions, and confinement effects of the n-heptane within the UiO-67-CH₃ pores. We hypothesize a similar effect for UiO-67-NH₂, where confinement of n-heptane near the linker amine groups likely strengthens the binding interactions induced by weak hydrogen bonding.¹⁷

The vibrational signature of MOF-analyte interactions

Complementary to TPD-MS, temperature-programmed FT-IR can provide detailed *in situ* information about the nature of the MOF-analyte interactions by monitoring changes in the MOF IR signature during (a) the adsorption process, (b) the heating process, and (c) after the removal of surface-bound species. The information encoded in the MOF vibrational signature is interpreted in order to determine the similarities and differences in interactions of the various analytes with the framework.

Acetone

In order to gain more fundamental insights into the interactions of acetone with the UiO-67 MOFs, we use *in situ* IR to monitor changes in the MOF IR signature during analyte uptake and as the sample is heated to the activation temperature. Initially, following ~1100 L acetone exposure at 100 K, several spectral features characteristic of crystalline acetone are observed in the IR difference spectra (Fig. S6).⁵⁰ For all MOFs, a peak near 1710 cm⁻¹ is assigned to the carbonyl stretching frequency of acetone, ν(C=O).⁵¹ This feature is redshifted (~11 cm⁻¹) relative to free acetone carbonyl, confirming multilayer acetone adsorption on the external MOF surface,⁵¹ in good agreement with the TPD-MS results. A table of relevant band assignments for the acetone features observed at 100 K for all UiO-67-X MOFs is provided in Table S1.

MOF-acetone interactions are recognized by changes in the MOF IR profile during heating from 100 to 473 K at 1 K s⁻¹

following acetone exposure (100 K), which we discuss using the unfunctionalized UiO-67 as the representative example. IR difference spectra, generated using a reference spectrum of the clean MOF at the same temperature, resolve the temperature-dependent acetone–MOF interactions by excluding any interference from heating effects on the pristine MOF's own IR features.²³

Upon acetone adsorption at 100 K [Fig. 2(a), black solid line], it is apparent that a small fraction of the acetone directly interacts with the μ_3 -OH groups on the Zr-node [viz., the negative $\nu(\mu_3\text{-OH})$ band at 3678 cm^{-1}] forming hydrogen bonds with the acetone carbonyl [viz., positive $\nu(\mu_3\text{-OH})_{\text{HB}}$ centered at 3450 cm^{-1}]. Two additional features near $\nu(\mu_3\text{-OH})_{\text{HB}}$ are also observed at

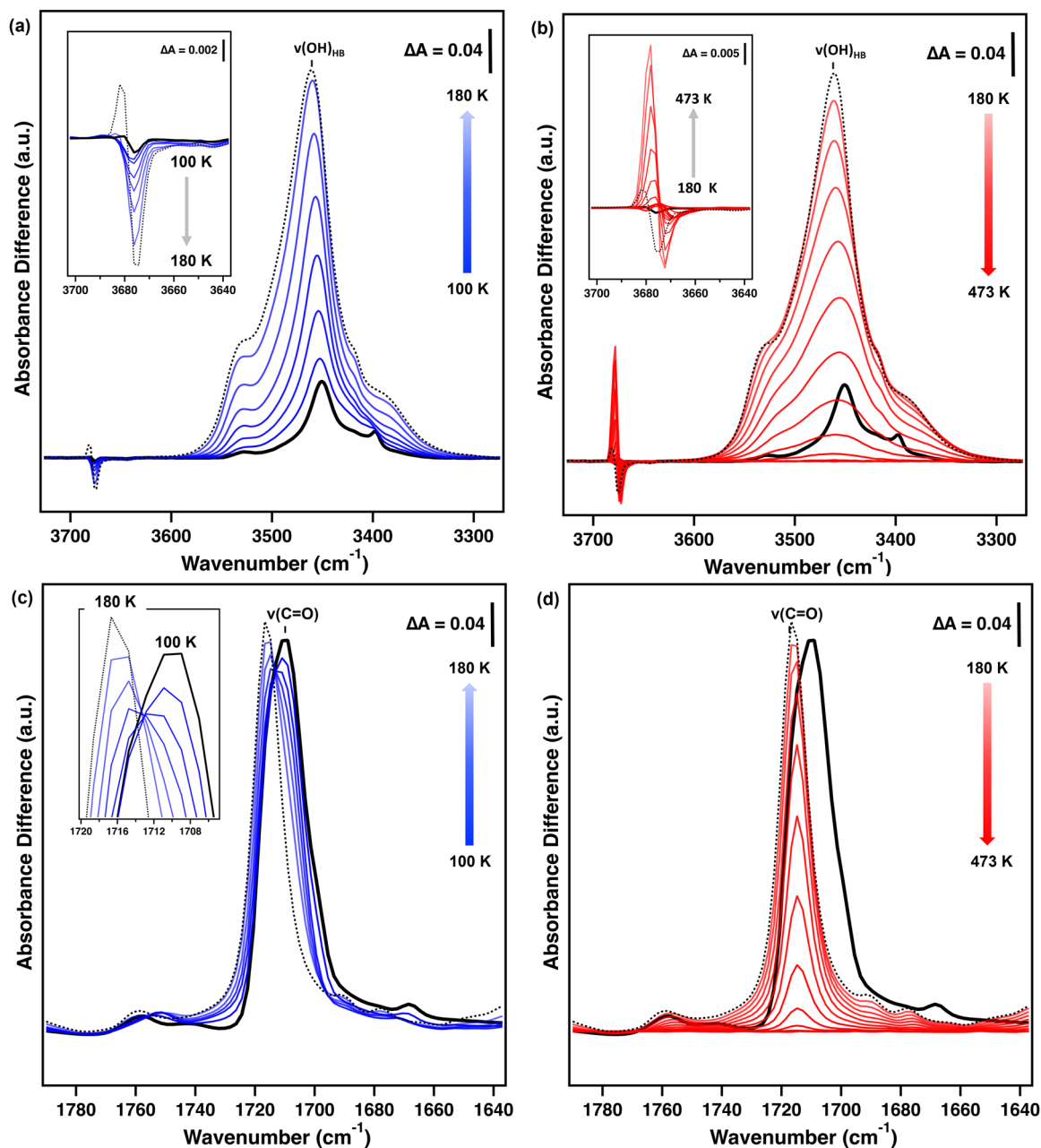


FIG. 2. TP-IR difference spectra acquired during heating UiO-67 from 100 to 473 K at ~ 1.0 K/s following 1100 L acetone exposure at 100 K. The evolution of hydrogen bonded species $\nu(\mu_3\text{-OH})_{\text{HB}}$ within the temperature regions (a) 100–180 K (blue) and (b) 180–473 K (red) where the inset highlights $\nu(\mu_3\text{-OH})_{\text{free}}$. The evolution of the acetone carbonyl stretch, $\nu(\text{C}=\text{O})$, within the temperature regions (c) 100–180 K (blue) and (d) 180–473 K (red). In all cases, the black dashed spectra correspond to the UiO-67 sample at 180 K.

3530 and 3398 cm^{-1} . The band at 3398 cm^{-1} is assigned to the first acetone carbonyl overtone stretch, $2\nu(\text{C}=\text{O})$.^{52,53} The band at 3530 cm^{-1} originates from a hydrogen bonded interaction between the acetone carbonyl and a small quantity of water that likely entered the UHV chamber from residual water remaining in the acetone dosing flask or from adsorbed in the UHV gas line. This assignment was guided by a previous report, which identified a feature at 3520 cm^{-1} to result acetone–water hydrogen bonding originating from water contamination in the IR signature of liquid “neat” acetone.⁵⁴

Acetone diffusion from the external crystallite surface into the internal pore environment is expected as the sample temperature is increased. Indeed, from 100 to 180 K [Fig. 2(a)], a decrease of the MOF $\nu(\mu_3\text{-OH})$ at 3678 cm^{-1} is accompanied by the growth of $\nu(\text{OH})_{\text{HB}}$ centered at 3450 cm^{-1} . This observation provides evidence that as the sample temperature is increased, acetone diffuses into the internal UiO-67 pore environment where majority of the $\mu_3\text{-OH}$ groups reside [Fig. 2(a)].⁵⁵ We note that the TPD-MS spectrum of acetone has a peak at ~ 180 K, at which point most weakly bound acetone has diffused from the external multilayer into the MOF crystallite. We suspect that the correlations between the TPD-MS and TP-IR spectra are indicative of the remaining acetone molecules being preferentially adsorbed at $\mu_3\text{-OH}$ sites.

Continued heating above 180 K [Fig. 2(b)] leads to the removal of hydrogen bonded acetone evidenced by the monotonic loss of $\nu(\mu_3\text{-OH})_{\text{HB}}$. As the acetone population in the framework decreases, there are fewer molecules available to hydrogen bond, leading to the reemergence of the isolated $\nu(\mu_3\text{-OH})$ signal. The complete disappearance of $\nu(\text{OH})_{\text{HB}}$ and full recovery of $\nu(\mu_3\text{-OH})$ are

observed by 320 K [Fig. 2(b)], consistent with the TPD-MS results.

The acetone carbonyl stretch, $\nu(\text{C}=\text{O})$, initially observed at 1710 cm^{-1} [Fig. 2(c) inset], is typically employed as a spectroscopic probe of the presence of acetone.⁵⁶ As the sample temperature is increased from 100 to 180 K [Fig. 2(c)], the $\nu(\text{C}=\text{O})$ band blueshifts and slightly (<10%) decreases in spectral intensity, reaching a minimum by 120 K, but then regains its initial intensity by 180 K. This intensity decrease with heating has been detected previously and was attributed to the change in phase from an amorphous solid (80 K) to an ordered (crystalline) phase (120 K) and finally to an isotropic phase (140 K).⁵⁷ Specifically, the $\nu(\text{C}=\text{O})$ band intensity is reported to decrease upon heating from 80–120 K and then recovers to its initial intensity with continued heating from 120–140 K.⁵⁷ Therefore, we attribute the observed intensity changes to confined acetone changing phase within the internal UiO-67 pore environment. The integrated intensity of both $\nu(\text{C}=\text{O})$ and $\nu(\text{CH})$ (Fig. 3) shows an increase between 100 and 180 K, while the TPD-MS spectrum [Fig. 1(a)] shows evidence of multilayer desorption, i.e., a decrease in total amount of adsorbate. The total integrated $\nu(\text{C}=\text{O})$ and $\nu(\text{CH})$ intensities are thus inconsistent with the amount of acetone present at the sample, i.e., the $\nu(\text{C}=\text{O})$ and $\nu(\text{CH})$ cross sections change following diffusion into UiO-67 and therefore defy the Beer–Lambert law.^{56,58} This suggests that the acetone $\nu(\text{C}=\text{O})$ and $\nu(\text{CH})$ modes cannot be trivially used as a metric of the quantity of acetone simultaneously on the exterior and interior of UiO-67, even in the limit of low coverage.²⁰ This increase in the acetone $\nu(\text{C}=\text{O})$ mode is surprising, as previous studies revealed a decrease in infrared cross sections following diffusion into a porous material, e.g., acetone diffused into single wall carbon nanotubes.⁵⁶ We suspect the

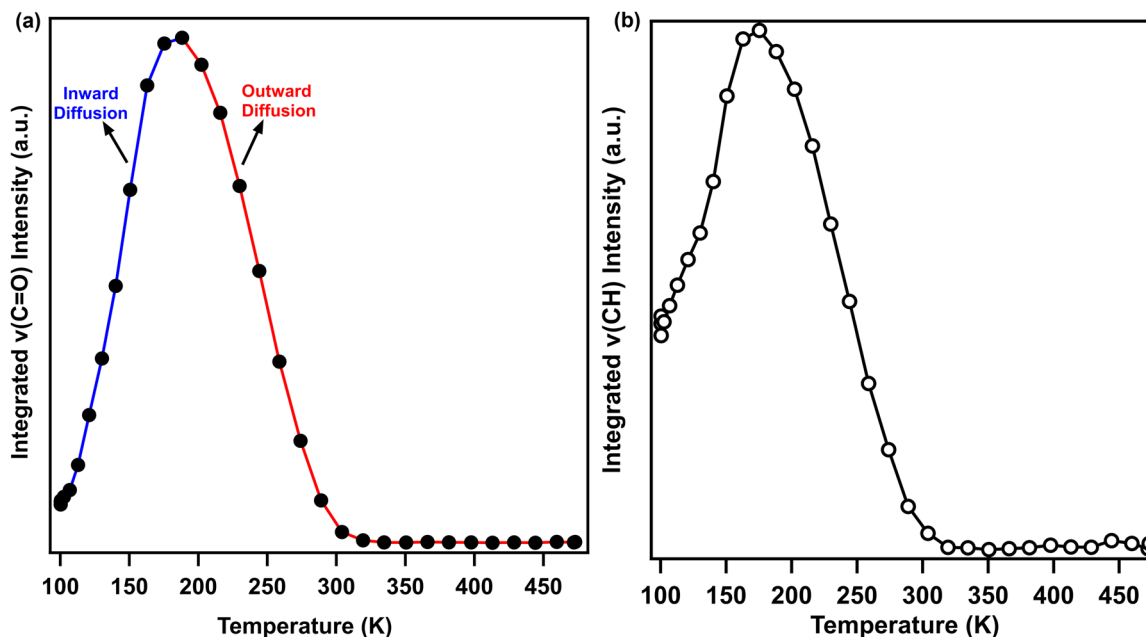


FIG. 3. Integrated intensity of acetone vibrational modes during heating of UiO-67 to 473 K at ~ 1.0 K/s following 1100 L exposure: (a) acetone $\nu(\text{C}=\text{O})$ modes and (b) acetone $\nu(\text{CH})$ modes.

growth in the $\nu(\text{C}=\text{O})$ integrated intensity is due to hydrogen bonding interactions, which increase the dipole moment along the $\text{C}=\text{O}$ bond, thus increasing the $\nu(\text{C}=\text{O}) \frac{\partial \bar{\mu}}{\partial Q}$ value when diffused into UiO-67, where $\bar{\mu}$ is an electric dipole moment and Q is a normal mode coordinate. Note that the IR intensity, I_{IR} , of an IR active normal mode is written as $I_{\text{IR}} \approx \left| \frac{\partial \bar{\mu}}{\partial Q} \right|^2$ under the electric dipole and harmonic oscillator approximations.⁵⁹

We note that no appreciable loss in $\nu(\text{C}=\text{O})$ intensity is observed until sample temperatures exceed 200 K [Figs. 2(c), 2(d), and 3(a)]; the gradual decrease of the $\nu(\text{C}=\text{O})$ integrated intensity following 200 K continues with the increasing temperature, and the feature completely disappears from the IR spectrum by 320 K [Figs. 2(d) and 3(a)]. This behavior occurs simultaneously with the loss of $\nu(\mu_3\text{-OH})_{\text{HB}}$ features and indicates that for temperatures above 200 K, acetone molecules diffuse out of the framework and desorb. The complete loss of the acetone $\nu(\text{C}=\text{O})$ and $\nu(\mu_3\text{-OH})_{\text{HB}}$ features as well as recovery of the initial clean MOF spectrum after heating to 473 K further support molecular physisorption of acetone evidenced by TPD-MS (Fig. S3).

Isopropanol

Upon exposure to ~ 1100 L of isopropanol at 100 K, several spectral features characteristic of crystalline isopropanol are observed in the IR difference spectra for unfunctionalized UiO-67 (Fig. 4). Isopropanol adsorption on the external crystallite surface is confirmed by the appearance of intrinsic $\nu(\text{CH})$ stretching modes at 2968, 2926, and 2880 cm^{-1} , which are redshifted relative to crystalline isopropanol at 120 K.⁴⁷ The asymmetric methyl C–H stretch $\nu(\text{CH})_{\text{as}}$ (2968 cm^{-1}) is the most intense of the intrinsic C–H isopropanol features. We note that the $\nu(\text{CH})$ oscillator intensities are nonlinear with concentration, deviating from Beer–Lambert's law [Fig. 4(b)]. While the general trend of decreasing $\nu(\text{CH})$ intensity is consistent with the TPD-MS spectrum, the decrease is not monotonic, suggesting that diffusion into the MOF changes $\frac{\partial \bar{\mu}}{\partial Q}$ of the $\nu(\text{CH})$ modes. Faraday shielding, primarily induced by image charges,⁶⁰ has been shown to affect infrared intensities for molecules diffused into single wall carbon nanotubes (SWCNTs).⁵⁶ However, the infrared intensity behavior reported here likely arises from hydrogen bonding and/or short-range interactions between the analyte and MOF moieties, as observed by McDonnell and co-workers.²⁰

The intensity changes in $\nu(\text{CH})$ indicate that, as the sample temperature is increased, diffusion of isopropanol molecules into the internal pore environment and desorption from the external crystallite increases. Unlike acetone, isopropanol can form hydrogen bonds with itself, acting as both a proton donor and acceptor, which complicates interpretation of its $\nu(\text{OH})$ region. It is generally reported that the hydrogen bonded aggregation state of alcohols decreases with the increasing temperature, where $\nu(\text{OH})_{\text{HB}}$ of highly ordered aggregates are observed at lower frequencies, as reported for isopropanol in argon matrices.^{61–63} As more thermal energy is provided to the system, isopropanol molecules break away from the multilayer and diffuse into the internal pores, revealed experimentally by a blueshift of the broad $\nu(\text{OH})_{\text{HB}}$ band centered 3240 cm^{-1} (100 K) and the evolution of several other distinct $\nu(\text{OH})$ bands at 3195, 3276, 3397, 3480, and 3600 cm^{-1} with heating (Fig. 4).

The $\nu(\text{OH})$ band at 3600 cm^{-1} evolves with the increasing temperature, changing only in intensity with no shift in frequency [Fig. 4(a)]. We assign this feature to the direct hydrogen-bonding interaction of isopropanol with the $\mu_3\text{-OH}$ groups of UiO-67, which we term $\nu(\mu_3\text{-OH})'_{\text{HB}}$. The transport of isopropanol into and out of UiO-67 during heating is tracked via the integrated intensity of $\nu(\mu_3\text{-OH})'_{\text{HB}}$. Quantitatively, the integrated intensity of $\nu(\mu_3\text{-OH})'_{\text{HB}}$ increases as a function of temperature up to ~ 220 K where it reaches maximum intensity, before decreasing in intensity with continued heating to 473 K [Fig. 4(b)]. We interpret this as the increasing population of isopropanol–MOF hydrogen bonds as molecules break off from the crystallite surface and diffuse into the internal pore environment of UiO-67 before reaching a critical point then diffusing out of the framework and desorbing [Fig. 4(a)]. Similar to acetone, there appears to be a peak in the TPD-MS spectrum at ~ 220 K, suggesting that the remaining isopropanol molecules are preferentially adsorbed at the high energy binding sites at 220 K. By 473 K, there is a complete disappearance of all isopropanol $\nu(\text{OH})$ modes, accompanied by the recovery of the MOF $\nu(\mu_3\text{-OH})$ mode, confirming that isopropanol interactions with UiO-67 are reversible.

n-heptane

Upon exposure of UiO-67 to ~ 1100 L n-heptane at 100 K, several features appear within the high wavenumber region of the infrared difference spectrum at 2849, 2870, 2916, 2951, and 3640 cm^{-1} [Fig. 5(a)], consistent with previous literature reports of n-alkane adsorption on UiO-66 and porous zeolites.^{17,64} The feature at 3640 cm^{-1} correlates with the disappearance of the intrinsic UiO-67 $\nu(\mu_3\text{-OH})$ mode at 3677 cm^{-1} , indicating that n-heptane adsorption at 100 K perturbs the local environment around the free $\mu_3\text{-OH}$ groups [black solid spectrum, Fig. 5(a)].¹⁷ This suggests that some n-heptane enters into the internal pores where it can interact with $\mu_3\text{-OH}$ groups upon adsorption at 100 K.

The diffusion of n-heptane into UiO-67 is recognized by changes in the $\nu(\mu_3\text{-OH})'_{\text{HB}}$ band at 3641 cm^{-1} as temperature is ramped from 100–473 K [Fig. 5(a)]. As the sample temperature is increased, $\nu(\mu_3\text{-OH})'_{\text{HB}}$ blueshifts and increases in intensity, reaching a maximum at 236 K [dashed spectra, Fig. 5(b)]. Continued heating above 236 K leads to the decay of $\nu(\mu_3\text{-OH})'_{\text{HB}}$, which completely disappears from the IR spectrum by 326 K and is accompanied by the recovery of the intrinsic $\nu(\mu_3\text{-OH})$ mode.

The normalized integrated intensities of $\nu(\mu_3\text{-OH})'_{\text{HB}}$ at 3641 cm^{-1} and $\nu(\text{CH})$ modes (2800–2978 cm^{-1}) provide insights into the transport of n-heptane during heating [Fig. 5(d)]. Tracking the loss in integrated intensity as a function of temperature determines the temperature range associated with the molecules leaving the MOF. Unlike acetone, we observe two steps in the loss of n-heptane $\nu(\text{CH})$ modes [open circles, Fig. 5(d)]. Between 130 and 170 K, a loss of $\sim 25\%$ of the adsorbed n-heptane molecules is observed, which is followed by a plateau region where no further loss of $\nu(\text{CH})$ modes is observed until the sample temperature exceeds 236 K. The initial loss between 130 and 170 K is in reasonable agreement with desorption from the initial, low temperature site ($T_{\text{des}} \sim 165$ K) observed in the TPD-MS spectrum [Fig. 1(c)].

Similar to acetone and isopropanol, the cross sections of the n-heptane $\nu(\text{CH})$ modes are affected by diffusion into UiO-67

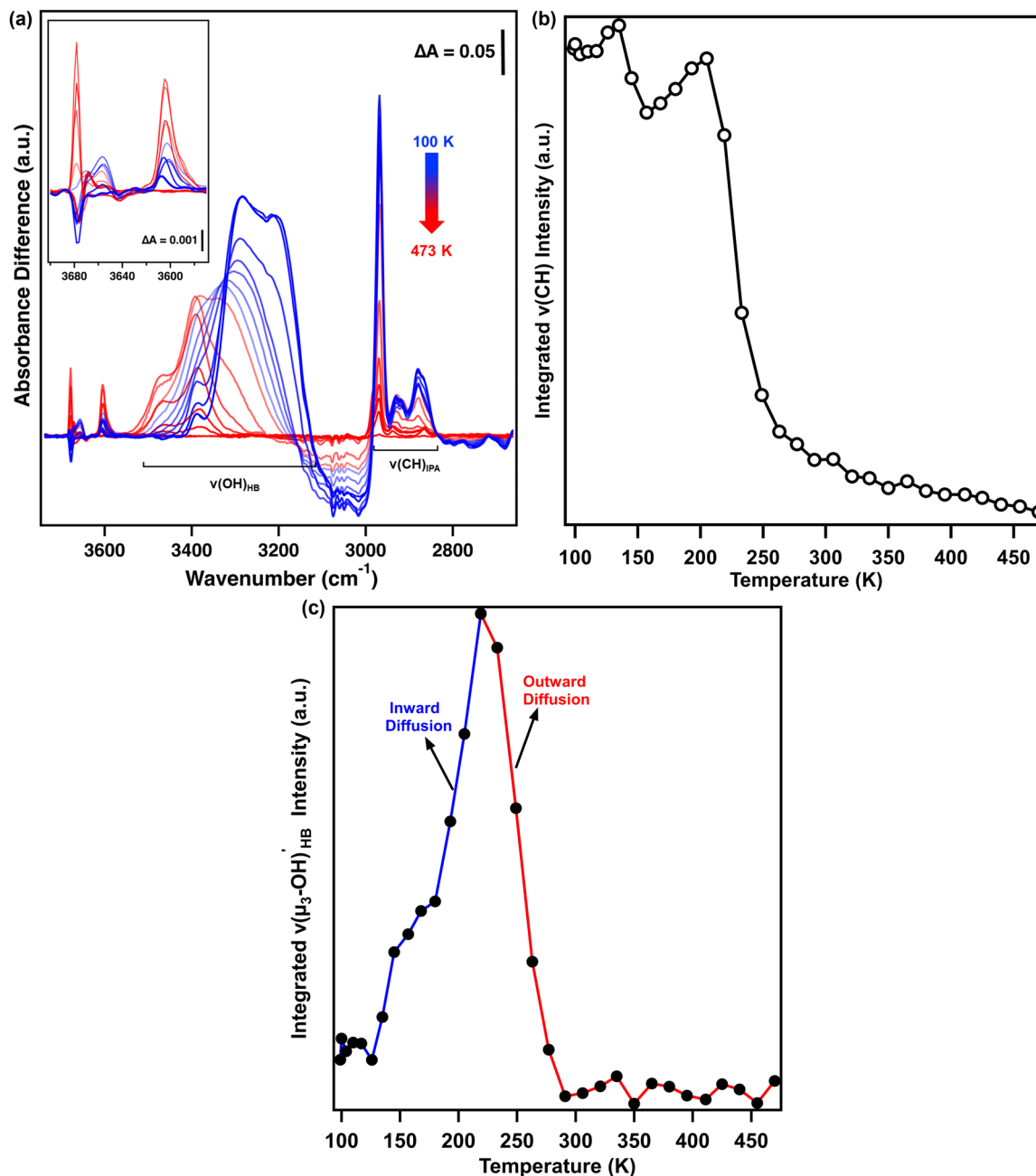


FIG. 4. TP-IR difference spectra acquired during heating UiO-67 from 100 to 473 K at ~ 1.0 K/s following 1100 L isopropanol exposure at 100 K. (a) IR difference spectra collected *in situ* following exposure to ~ 1100 L of isopropanol and during heating at ~ 1.0 K/s, revealing the temperature dependent MOF–isopropanol interactions for UiO-67 from 100 K (dark blue) to 473 K (dark red). Difference spectra were generated by subtracting each IR spectrum with a spectrum of the clean MOF at the same temperature. (b) Integrated infrared intensity of intrinsic isopropanol $\nu(\text{CH})$ during heating. (c) Integrated infrared intensity of $\nu(\mu_3\text{-OH})_{\text{HB}}$ during heating.

[Fig. 5(d)]. The loss of $\nu(\text{CH})$ slows considerably between 170 and 236 K, as the intensity of the $\nu(\mu_3\text{-OH})_{\text{HB}}$ mode at 3641 cm^{-1} continues to increase, suggesting diffusion into the MOF crystallite coupled with desorption [Fig. 1(c)]. This is inconsistent with the TPD-MS spectrum [Fig. 1(c)], which clearly depicts the loss of

n-heptane between 200 and 236 K. Notably, at the onset of the second loss in $\nu(\text{CH})$ at 236 K, the intensity of $\nu(\mu_3\text{-OH})_{\text{HB}}$ reaches a maximum [Fig. 5(d)]. Continued heating above 236 K leads to the loss of both $\nu(\text{CH})$ and $\nu(\mu_3\text{-OH})_{\text{HB}}$ modes, proceeding at similar rates as indicated by the slopes of the integrated area curves. By

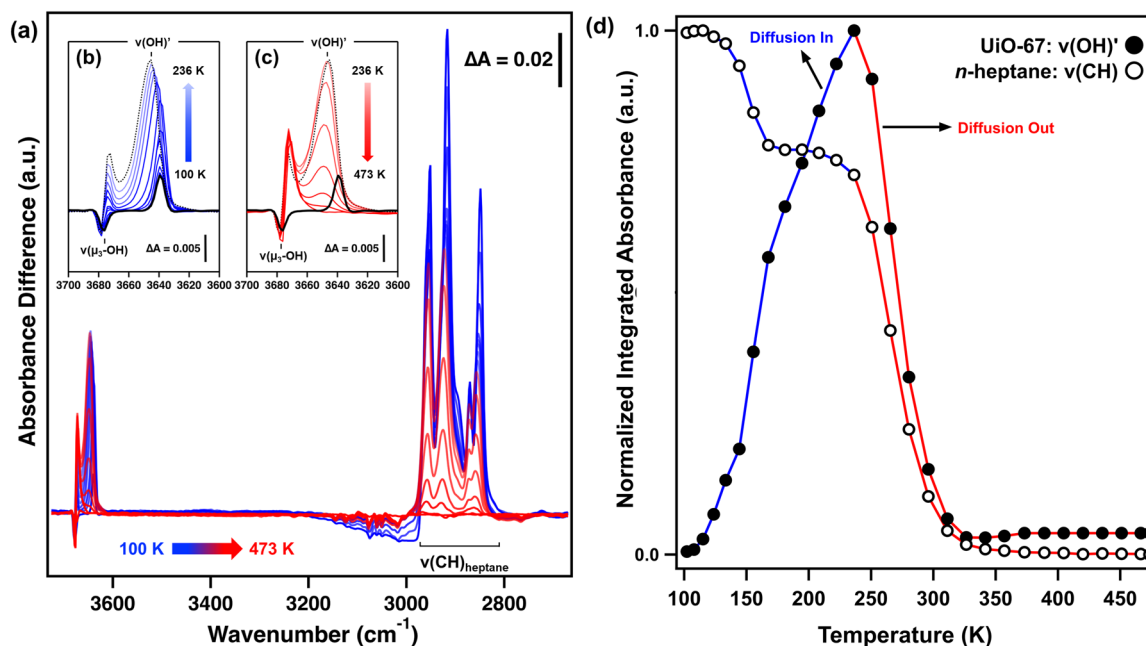


FIG. 5. TP-IR difference spectra of UiO-67 collected during heating from 100 to 473 K at ~ 1.0 K/s following exposure to ~ 1100 L of n-heptane at 100 K (black solid spectrum) showing (a) perturbation of $\nu(\mu_3\text{-OH})$ due to n-heptane diffusion into the MOF interior. The insets show heating induced effects within the temperature regions (b) 100–236 K (blue) and (c) 236–473 K (red). The black dashed spectra in the insets correspond to the sample at 236 K. Difference spectra were generated by subtracting each IR spectrum with a spectrum of the clean MOF at the same temperature. (d) Temperature-dependent evolution of n-heptane interactions with UiO-67 tracking the integrated absorbance of the MOF $\nu(\text{OH})'$ (closed circles) and the intrinsic n-heptane $\nu(\text{CH})$ modes between 2968 and 2880 cm^{-1} (open circles).

326 K, all n-heptane has desorbed from the framework and the initial state of the clean MOF is recovered, indicating that interactions with n-heptane are reversible.

Comparison of analyte interactions with UiO-67

By comparing the three different analyte interactions with unfunctionalized UiO-67, we can identify if analyte polarity impacts the binding strength. The polarity index is defined as “the ability of the solvent to interact with various test solutes,”⁶⁵ which scales with increasing polarity. For the analytes reported here, the reported polarity index values are n-heptane (0.1), isopropanol (3.9), and acetone (5.1).^{65,66}

TPD-MS provides insights into the accessibility and strength of binding sites with the MOF. Using UiO-67 as a representative example, we compare the binding preferences of ~ 1100 L exposure of acetone, isopropanol, and n-heptane (Fig. 1). Several features are observed in each of the TPD-MS spectra, indicating that all analytes have sufficient mobility upon adsorption and during the temperature ramp to access multiple binding sites within the UiO-67 MOF (Fig. 1). A low temperature feature, close to their respective sublimation temperatures, is observed for all analytes, which we attributed to molecules desorbing from a condensed layer on the external crystallite surface. The highest temperature feature observed in the TPD-MS is reflective of the highest energy binding site of the MOF, which yields a relative trend in desorption energy as acetone (5.1) < n-heptane (0.1) \approx isopropanol

(3.9) for UiO-67. The observed trend in binding strength, at least in the limit of low coverage, suggests that solvent polarity is not a useful indicator for predicting the strength of MOF–analyte binding interactions. Instead, the intrinsic functionality of the analyte plays an important role in the binding interactions with the MOF (*vide infra*).

The effects of analyte functionality on the interactions with the $\mu_3\text{-OH}$ groups of UiO-67 are reflected in the infrared spectra collected immediately following ~ 1100 L analyte exposure at 100 K (blue curve, Fig. 6) and at elevated temperatures, e.g., 200 K (red curve, Fig. 6). Isopropanol, a simple alcohol, differs structurally from acetone at the central carbon, which bears a single bond to oxygen (C–OH) rather than a double bond (C=O). Although these molecules are structurally similar, this slight modification at the central carbon contributes significantly to differences in their properties. With respect to hydrogen bonding, acetone can only act as a proton acceptor, whereas isopropanol can act as both a proton donor and acceptor, enabling the possibility of multiple, simultaneous hydrogen bonding interactions. This difference is reflected in the UiO-67 IR spectra collected following ~ 1100 L analyte exposure at 100 K and at 200 K (Fig. 4), where the relative strength of the hydrogen bonding interactions is assessed by the position of the hydrogen-bonded OH signal; the more redshifted the $\nu(\text{OH})_{\text{HB}}$ signal, the stronger the analyte–MOF hydrogen bond. At 100 K, the broad $\nu(\mu_3\text{-OH})_{\text{HB}}$ signal for acetone (3545–3370 cm^{-1}) is blueshifted relative to the broad $\nu(\text{OH})_{\text{HB}}$ for isopropanol (3370–3130 cm^{-1}), signifying that isopropanol forms stronger, and

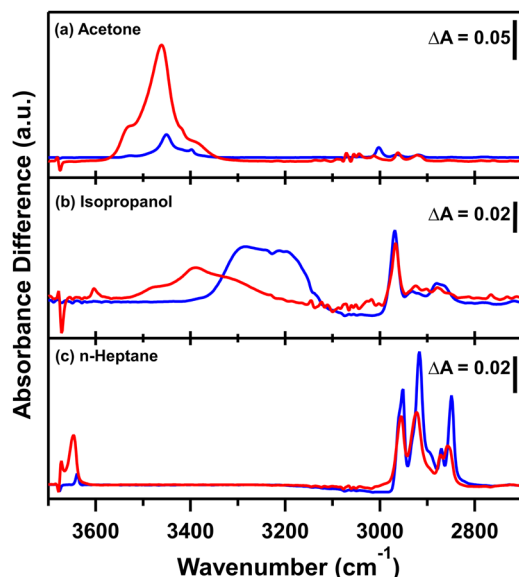


FIG. 6. FT-IR spectra of UiO-67 interacting with (a) acetone, (b) isopropanol, and (c) n-heptane, immediately following ~ 1100 L analyte exposure at 100 K (blue) and during heating at 200 K (red). All spectra are baseline corrected; a spectrum of the clean MOF at 100 K (blue) and 200 K (red) was subtracted from each corresponding spectrum at 100 or 200 K, respectively.

likely multiple, hydrogen bonds with the framework. However, we recognize that for isopropanol, a majority of the $\nu(\text{OH})_{\text{HB}}$ signal at 100 K is associated with the condensed network of isopropanol–isopropanol hydrogen bonding interactions, which is significantly reduced at higher sample temperatures as isopropanol diffuses into the internal pores of the MOF. At 200 K, $\nu(\text{OH})_{\text{HB}}$ for both isopropanol and acetone blueshift, indicating a weakening of their hydrogen bonded interactions, yet $\nu(\text{OH})_{\text{HB}}$ for isopropanol generally remains redshifted relative to acetone. This is consistent with density functional theory calculations, suggesting that isopropanol binds more strongly to μ_3 -OH groups relative to acetone in UiO-66.^{49,55} Moreover, UiO-67 interaction with isopropanol has a more pronounced effect on the MOF μ_3 -OH groups than acetone, where a large decrease in intensity is observed at 200 K. The infrared spectra of adsorbed isopropanol and n-heptane suggest that C–H functionalities induce a subtle redshift in $\nu(\mu_3\text{-OH})$ ($\Delta\tilde{\nu} \approx 20\text{--}80\text{ cm}^{-1}$), which could be used as an indicator for the binding orientation of molecules due to the presence of CH groups.¹⁷ We suspect that contributions from attractive interactions with the π -system of the organic linker could explain the large binding energies extrapolated from the TPD-MS spectra.^{49,67,68} Ultimately, our results suggest that analyte functionality may be more important than the polarity of the solvent, expected through analysis of possible intermolecular forces between these molecules and UiO-67.

CONCLUSIONS

A combination of temperature programmed desorption-mass spectrometry and *in situ* FT-IR spectroscopy under UHV

conditions has revealed the interactions of simple solvents with the UiO-67 series of MOFs. In the limit of low coverage, TPD-MS results provide insights into the accessibility of binding sites, providing evidence that both MOF and analyte functionalities influence relative binding strengths. *In situ* FT-IR provides complementary insights by enabling the interpretation of analyte binding preferences and reveals that regardless of polarity, both polar and non-polar analytes can access the internal pore environment and interact with the MOF μ_3 -OH groups. It is observed that the $\nu(\text{CH})$ infrared cross sections of acetone, isopropanol, and n-heptane possess nonlinear behavior, changing following diffusion into UiO-67. This deviation from the Beer–Lambert law introduces non-trivial effects which must be accounted for to understand molecular transport in and out of UiO-67. Complementary TPD-MS and FT-IR experiments show that the analyte functionality dominates MOF–guest interactions, as opposed to other chemical properties, such as polarity. TPD-MS results show that polar analytes interact with UiO-67-NH₂ more strongly than UiO-67 and UiO-67-CH₃. Redshifts in $\nu(\mu_3\text{-OH})$ are employed to differentiate between analyte binding sites in UiO-67. It is observed that both nonpolar, aprotic and polar, protic analytes interact with μ_3 -OH groups via CH₃ groups. For hydrogen bonded species, a more redshifted $\nu(\mu_3\text{-OH})$ ($\Delta\tilde{\nu} > 300\text{ cm}^{-1}$) correlates to a larger desorption energy, providing a useful metric for understanding preferred binding interactions in UiO-67. Overall, the spectroscopic knowledge gleaned from this study will provide insights into how more complex species interact with differing MOF moieties.

SUPPLEMENTARY MATERIAL

See the supplementary material for material and analyte characterization, discussion on molecular physisorption, discussion on relative analyte coverage, additional TPD-MS and FT-IR spectra, and vibrational mode assignments.

ACKNOWLEDGMENTS

The authors thank Avery Green and Carl Ventrice for providing LabVIEW code to run TPD experiments. M.C.B., L.C., and R.P.M. received support from the Temple University College of Science and Technology Undergraduate Research Program. M.C.B., L.C., and R.P.M. thank Edwin Ovalle and Paul Svitak for helpful discussions. R.P.M. gratefully acknowledges the National Science Foundation (NSF) (Grant No. DUE-1643874) and the NSF Graduate Research Fellowship Program (Grant No. DGE-2137424) for support. This project received support from the Defense Threat Reduction Agency (DTRA) (Grant No. HDTRA1-21-1-0019).

AUTHOR DECLARATIONS

Conflict of Interest

The authors have no conflicts to disclose.

Author Contributions

I.G., M.C.B., and R.P.M. contributed equally to this work.

The manuscript was written through contributions of all authors. All authors have given approval to the final version of the manuscript.

Isabella Goodenough: Conceptualization (equal); Data curation (equal); Formal analysis (equal); Investigation (equal); Methodology (equal); Supervision (equal); Visualization (equal); Writing – original draft (equal); Writing – review & editing (equal). **Mikaela C. Boyanich:** Conceptualization (equal); Data curation (equal); Formal analysis (equal); Investigation (equal); Methodology (equal); Visualization (equal); Writing – original draft (equal); Writing – review & editing (equal). **Ryan P. McDonnell:** Conceptualization (equal); Data curation (equal); Formal analysis (equal); Investigation (equal); Methodology (equal); Visualization (equal); Writing – original draft (equal); Writing – review & editing (equal). **Lauren Castellana:** Conceptualization (equal); Data curation (equal); Formal analysis (equal); Investigation (equal); Methodology (equal); Writing – review & editing (equal). **Venkata Swaroopa Datta Devulapalli:** Methodology (equal); Supervision (equal); Visualization (equal); Writing – review & editing (equal). **Tian-Yi Luo:** Resources (equal). **Prasenjit Das:** Resources (equal). **Mélanie Richard:** Conceptualization (equal); Data curation (equal); Formal analysis (equal); Investigation (equal); Methodology (equal); Supervision (equal); Visualization (equal); Writing – review & editing (equal). **Nathaniel L. Rosi:** Funding acquisition (equal); Resources (equal); Supervision (equal); Writing – review & editing (equal). **Eric Borguet:** Conceptualization (equal); Formal analysis (equal); Funding acquisition (equal); Investigation (equal); Methodology (equal); Project administration (equal); Supervision (equal); Writing – original draft (equal); Writing – review & editing (equal).

DATA AVAILABILITY

The data that support the findings of this study are available from the corresponding author upon reasonable request.

REFERENCES

- M. Kumai, A. Koizumi, K. Saito, H. Sakurai, T. Inoue, Y. Takeuchi, I. Hara, M. Ogata, T. Matsushita, and M. Ikeda, “A nationwide survey on organic solvent components in various solvent products: Part 2. Heterogeneous products such as paints, inks and adhesives,” *Ind. Health* **21**(3), 185–197 (1983).
- N. A. Khan, Z. Hasan, and S. H. Jhung, “Adsorptive removal of hazardous materials using metal-organic frameworks (MOFs): A review,” *J. Hazard. Mater.* **244–245**, 444–456 (2013).
- Y. Wu, D. F. Liu, Y. B. Wu, Y. Qian, and H. X. Xi, “Effect of electrostatic properties of IRMOFs on VOCs adsorption: A density functional theory study,” *Adsorption* **20**(5-6), 777–788 (2014).
- N. S. Bobbitt, M. L. Mendonca, A. J. Howarth, T. Islamoglu, J. T. Hupp, O. K. Farha, and R. Q. Snurr, “Metal-organic frameworks for the removal of toxic industrial chemicals and chemical warfare agents,” *Chem. Soc. Rev.* **46**(11), 3357–3385 (2017).
- J. B. DeCoste, G. W. Peterson, H. Jasuja, T. G. Glover, Y. G. Huang, and K. S. Walton, “Stability and degradation mechanisms of metal-organic frameworks containing the $Zr_6O_4(OH)_4$ secondary building unit,” *J. Mater. Chem. A* **1**(18), 5642–5650 (2013).
- C. Halliday and T. A. Hatton, “Sorbers for the capture of CO_2 and other acid gases: A review,” *Ind. Eng. Chem. Res.* **60**(26), 9313–9346 (2021).
- J. DeCoste and G. Peterson, “Metal-organic frameworks for air purification of toxic chemicals,” *Chem. Rev.* **114**(11), 5695–5727 (2014).
- S. Chavan, J. G. Vitillo, D. Gianolio, O. Zavorotynska, B. Civalleri, S. Jakobsen, M. H. Nilsen, L. Valenzano, C. Lamberti, K. P. Lillerud, and S. Bordiga, “ H_2 storage in isostructural UiO-67 and UiO-66 MOFs,” *Phys. Chem. Chem. Phys.* **14**(5), 1614–1626 (2012).
- Y. Bai, Y. B. Dou, L. H. Xie, W. Rutledge, J. R. Li, and H. C. Zhou, “Zr-based metal-organic frameworks: Design, synthesis, structure, and applications,” *Chem. Soc. Rev.* **45**(8), 2327–2367 (2016).
- N. Li, J. Xu, R. Feng, T. L. Hu, and X. H. Bu, “Governing metal-organic frameworks towards high stability,” *Chem. Commun.* **52**(55), 8501–8513 (2016).
- A. M. Ploskonka and J. B. DeCoste, “Tailoring the adsorption and reaction chemistry of the metal-organic frameworks UiO-66, UiO-66-NH₂, and HKUST-1 via the incorporation of molecular guests,” *ACS Appl. Mater. Interfaces* **9**(25), 21579–21585 (2017).
- M. Linders, P. Baak, and J. van Bokhoven, “Exploratory investigation of the risk of desorption from activated carbon filters in respiratory protective devices,” *Ind. Eng. Chem. Res.* **46**(12), 4034–4039 (2007).
- A. J. Howarth, Y. Y. Liu, P. Li, Z. Y. Li, T. C. Wang, J. Hupp, and O. K. Farha, “Chemical, thermal and mechanical stabilities of metal-organic frameworks,” *Nat. Rev. Mater.* **1**(3), 15018 (2016).
- L. Valenzano, B. Civalleri, S. Chavan, S. Bordiga, M. H. Nilsen, S. Jakobsen, K. P. Lillerud, and C. Lamberti, “Disclosing the complex structure of UiO-66 metal organic framework: A synergic combination of experiment and theory,” *Chem. Mater.* **23**(7), 1700–1718 (2011).
- J. H. Cavka, S. Jakobsen, U. Olsbye, N. Guillou, C. Lamberti, S. Bordiga, and K. P. Lillerud, “A new zirconium inorganic building brick forming metal organic frameworks with exceptional stability,” *J. Am. Chem. Soc.* **130**(42), 13850–13851 (2008).
- R. W. Morrison, “Overview of current collective protection filtration technology,” in *NBC Defense Collective Protection Conference* (Guild Associates Inc, Baltimore, 2002).
- C. H. Sharp, J. Abelard, A. M. Plonka, W. W. Guo, C. L. Hill, and J. R. Morris, “Alkane-OH hydrogen bond formation and diffusion energetics of n-butane within UiO-66,” *J. Phys. Chem. C* **121**(16), 8902–8906 (2017).
- J. P. Ruffley, I. Goodenough, T. Y. Luo, M. Richard, E. Borguet, N. L. Rosi, and J. K. Johnson, “Design, synthesis, and characterization of metal-organic frameworks for enhanced sorption of chemical warfare agent simulants,” *J. Phys. Chem. C* **123**(32), 19748–19758 (2019).
- V. Swaroopa Datta Devulapalli, R. P. McDonnell, J. P. Ruffley, P. B. Shukla, T. Y. Luo, M. L. De Souza, P. Das, N. L. Rosi, J. Karl Johnson, and E. Borguet, “Identifying UiO-67 metal-organic framework defects and binding sites through ammonia adsorption,” *ChemSuschem* **15**(1), e202102217 (2022).
- R. P. McDonnell, V. S. D. Devulapalli, T. H. Choi, L. McDonnell, I. Goodenough, P. Das, N. L. Rosi, J. K. Johnson, and E. Borguet, “Anomalous infrared intensity behavior of acetonitrile diffused into UiO-67,” *Chem. Mater.* **35**(21), 8827–8839 (2023).
- S. Kwon, R. Vidic, and E. Borguet, “The effect of surface chemical functional groups on the adsorption and desorption of a polar molecule, acetone, from a model carbonaceous surface, graphite,” *Surf. Sci.* **522**(1–3), 17–26 (2003).
- X. Feng, C. Matrangola, R. Vidic, and E. Borguet, “A vibrational spectroscopic study of the fate of oxygen-containing functional groups and trapped CO_2 in single-walled carbon nanotubes during thermal treatment,” *J. Phys. Chem. B* **108**(52), 19949–19954 (2004).
- I. Goodenough, V. S. D. Devulapalli, W. Xu, M. C. Boyanich, T.-Y. Luo, M. De Souza, M. Richard, N. L. Rosi, and E. Borguet, “Interplay between intrinsic thermal stability and expansion properties of functionalized UiO-67 metal-organic frameworks,” *Chem. Mater.* **33**(3), 910–920 (2021).
- P. M. Donaldson, R. F. Howe, A. P. Hawkins, M. Towrie, and G. M. Greetham, “Ultrafast 2D-IR spectroscopy of intensely optically scattering pelleted solid catalysts,” *J. Chem. Phys.* **158**(11), 114201 (2023).
- P. A. Redhead, “Thermal desorption of gases,” *Vacuum* **12**(4), 203–211 (1962).
- A. M. de Jong and J. W. Niemantsverdriet, “Thermal desorption analysis: Comparative test of ten commonly applied procedures,” *Surf. Sci.* **233**(3), 355–365 (1990).
- E. Tomkova, “TDS spectra analysis,” *Surf. Sci.* **351**(1–3), 309–318 (1996).
- K. A. Fichthorn and R. A. Miron, “Thermal desorption of large molecules from solid surfaces,” *Phys. Rev. Lett.* **89**(19), 196103 (2002).

- ²⁹S. L. Tait, Z. Dohnalek, C. T. Campbell, and B. D. Kay, "n-alkanes on MgO(100). II. Chain length dependence of kinetic desorption parameters for small n-alkanes," *J. Chem. Phys.* **122**(16), 164708 (2005).
- ³⁰M. Tylinski, R. S. Smith, and B. D. Kay, "Structure and desorption kinetics of acetonitrile thin films on Pt(111) and on graphene on Pt(111)," *J. Phys. Chem. C* **124**(4), 2521–2530 (2020).
- ³¹M. Minissale, Y. Aikawa, E. Bergin, M. Bertin, W. A. Brown, S. Cazaux, S. B. Charnley, A. Coutens, H. M. Cuppen, V. Guzman *et al.*, "Thermal desorption of interstellar ices: A review on the controlling parameters and their implications from snowlines to chemical complexity," *ACS Earth Space Chem.* **6**(3), 597–630 (2022).
- ³²H. Eyring, "The activated complex in chemical reactions," *J. Chem. Phys.* **3**(2), 107–115 (1935).
- ³³D. A. McQuarrie, *Statistical Mechanics* (University Science Books, 2000).
- ³⁴J. M. Gottfried, E. K. Vestergaard, P. Bera, and C. T. Campbell, "Heat of adsorption of naphthalene on Pt(111) measured by adsorption calorimetry," *J. Phys. Chem. B* **110**(35), 17539–17545 (2006).
- ³⁵H. Goldstein, C. P. Poole, and J. L. Safko, *Classical Mechanics* (Addison Wesley, 2002).
- ³⁶M. J. Wilhelm, T. J. Johnson, and T. L. Myers, "Disentangling the confounding spectroscopy of C₁ molecules: Without symmetry as a guide, everything is allowed," *AIP Adv.* **13**(5), 051133 (2023).
- ³⁷P. Groner, E. Herbst, F. C. De Lucia, B. J. Drouin, and H. Mader, "Rotational spectrum of acetone, CH₃COCH₃, in the first torsional excited state," *J. Mol. Struct.* **795**(1–3), 173–178 (2006).
- ³⁸A. Maeda, I. R. Medvedev, F. C. De Lucia, E. Herbst, and E. Herbst, "The millimeter- and submillimeter-wave spectrum of iso-propanol [(CH₃)₂CHOH]," *Astrophys. J., Suppl. Ser.* **166**(2), 650–658 (2006).
- ³⁹K. N. Kirschner, W. Heiden, and D. Reith, "Small alcohols revisited: CCSD(T) relative potential energies for the minima, first- and second-order saddle points, and torsion-coupled surfaces," *Acs Omega* **3**(1), 419–432 (2018).
- ⁴⁰A. Wolfram, Q. Tariq, C. C. Fernandez, M. Muth, M. Gurrath, D. Wechsler, M. Franke, F. J. Williams, H. P. Steinruck, B. Meyer *et al.*, "Adsorption energies of porphyrins on MgO(100): An experimental benchmark for dispersion-corrected density-functional theory," *Surf. Sci.* **717**, 121979 (2022).
- ⁴¹D. Kazachkin, Y. Nishimura, S. Irle, K. Morokuma, R. D. Vidic, and E. Borguet, "Interaction of acetone with single wall carbon nanotubes at cryogenic temperatures: A combined temperature programmed desorption and theoretical study," *Langmuir* **24**(15), 7848–7856 (2008).
- ⁴²S. Kwon, J. Russell, X. C. Zhao, R. D. Vidic, J. K. Johnson, and E. Borguet, "Combined experimental and theoretical investigation of polar organic adsorption/desorption from model carbonaceous surfaces: Acetone on graphite," *Langmuir* **18**(7), 2595–2600 (2002).
- ⁴³D. J. Burke, A. J. Wolff, J. L. Edridge, and W. A. Brown, "The adsorption and desorption of ethanol ices from a model grain surface," *J. Chem. Phys.* **128**(10), 104702 (2008).
- ⁴⁴S. D. Green, A. S. Bolina, R. Chen, M. P. Collings, W. A. Brown, and M. R. S. McCoustra, "Applying laboratory thermal desorption data in an interstellar context: Sublimation of methanol thin films," *Mon. Not. R. Astron. Soc.* **398**(1), 357–367 (2009).
- ⁴⁵J. E. Schaff and J. T. Roberts, "Toward an understanding of the surface chemical properties of ice: Differences between the amorphous and crystalline surfaces," *J. Phys. Chem.* **100**(33), 14151–14160 (1996).
- ⁴⁶J. Goering, E. Kadossov, and U. Burghaus, "Adsorption kinetics of alcohols on single-wall carbon nanotubes: An ultrahigh vacuum surface chemistry study," *J. Phys. Chem. C* **112**(27), 10114–10124 (2008).
- ⁴⁷S. A. Ayling, D. J. Burke, T. L. Salter, and W. A. Brown, "Desorption and crystallisation of binary 2-propanol and water ices adsorbed on graphite," *RSC Adv.* **7**, 51621 (2017).
- ⁴⁸Y. An, A. Kleinhammes, P. Doyle, E. Y. Chen, Y. Song, A. J. Morris, B. Gibbons, M. Cai, J. K. Johnson, P. B. Shukla *et al.*, "In situ nuclear magnetic resonance investigation of molecular adsorption and kinetics in metal-organic framework UiO-66," *J. Phys. Chem. Lett.* **12**(2), 892–899 (2021).
- ⁴⁹C. V. Mhatre, J. J. Wardzala, P. B. Shukla, M. Agrawal, and J. K. Johnson, "Calculation of self, corrected, and transport diffusivities of isopropyl alcohol in UiO-66," *Nanomaterials* **13**(11), 1793 (2023).
- ⁵⁰R. L. Hudson, P. A. Gerakines, and R. F. Ferrante, "IR spectra and properties of solid acetone, an interstellar and cometary molecule," *Spectrochim. Acta, Part A* **193**, 33–39 (2018).
- ⁵¹S. W. Han and K. Kim, "Infrared matrix isolation study of acetone and methanol in solid argon," *J. Phys. Chem.* **100**(43), 17124–17132 (1996).
- ⁵²W. Hagen, A. G. G. M. Tielens, and J. M. Greenberg, "A laboratory study of the infrared spectra of interstellar ices," *Astron. Astrophys., Suppl. Ser.* **51**, 389–416 (1983).
- ⁵³J. Guan, Y. Hu, M. Xie, and E. R. Bernstein, "Weak carbonyl-methyl intermolecular interactions in acetone clusters explored by IR plus VUV spectroscopy," *Chem. Phys.* **405**, 117–123 (2012).
- ⁵⁴J.-J. Max and C. Chapados, "Infrared spectroscopy of acetone–water liquid mixtures. I. Factor analysis," *J. Chem. Phys.* **119**, 5632–5643 (2003).
- ⁵⁵J. J. Wardzala, J. P. Ruffley, I. Goodenough, A. M. Schmidt, P. B. Shukla, X. Wei, A. Bagussetty, M. De Souza, P. Das, D. J. Thompson *et al.*, "Modeling of diffusion of acetone in UiO-66," *J. Phys. Chem. C* **124**(52), 28469–28478 (2020).
- ⁵⁶D. V. Kazachkin, Y. Nishimura, H. A. Witek, S. Irle, and E. Borguet, "Dramatic reduction of IR vibrational cross sections of molecules encapsulated in carbon nanotubes," *J. Am. Chem. Soc.* **133**(21), 8191–8198 (2011).
- ⁵⁷S. Shin, H. Kang, J. S. Kim, and H. Kang, "Phase transitions of amorphous solid acetone in confined geometry investigated by reflection absorption infrared spectroscopy," *J. Phys. Chem. B* **118**(47), 13349–13356 (2014).
- ⁵⁸E. Borguet and H. L. Dai, "Site-specific properties and dynamical dipole coupling of CO molecules adsorbed on a vicinal Cu(100) surface," *J. Chem. Phys.* **101**(10), 9080–9095 (1994).
- ⁵⁹E. B. Wilson, J. C. Decius, and P. C. Cross, *Molecular Vibrations: The Theory of Infrared and Raman Vibrational Spectra* (Dover Publications, 1980).
- ⁶⁰J. D. Jackson, *Classical Electrodynamics* (Wiley, 1998).
- ⁶¹P. Lalanne, J. M. Andanson, J.-C. Soetens, T. Tassaing, Y. Danten, and M. Besnard, "Hydrogen bonding in supercritical ethanol assessed by infrared and Raman spectroscopies," *J. Phys. Chem. A* **108**, 3902–3909 (2004).
- ⁶²V. Balevicius, V. Sablinskas, I. Doroshenko, and V. Pogorelov, "Propanol clustering in argon matrix: 2D FTIR correlation spectroscopy," *Ukr. J. Phys.* **56**(8), 855–860 (2022).
- ⁶³N. Sugawara, P.-J. Hsu, A. Fujii, and J.-L. Kuo, "Competition between hydrogen bonds and van der Waals forces in intermolecular structure formation of protonated branched-chain alcohol clusters," *Phys. Chem. Chem. Phys.* **20**(39), 25482–25494 (2018).
- ⁶⁴Y.-H. Yeh, R. J. Gorte, S. Rangarajan, and M. Mavrikakis, "Adsorption of small alkanes on ZSM-5 zeolites: Influence of brønsted sites," *J. Phys. Chem. C* **120**(22), 12132–12138 (2016).
- ⁶⁵Summary of Key Physical Data for Solvents. Fisher Scientific UK Ltd., 2021. <https://www.fishersci.co.uk/gb/en/scientific-products/technical-tools/summary-key-physical-data-solvents.html> (accessed July 22, 2021).
- ⁶⁶L. R. Snyder, "Classification of the solvent properties of common liquids," *J. Chromatogr. A* **92**(2), 223–230 (1974).
- ⁶⁷S. G. Olesen and S. Hammerum, "Hydrogen bonding to alkanes: Computational evidence," *J. Phys. Chem. A* **113**(27), 7940–7944 (2009).
- ⁶⁸P. B. Shukla and J. K. Johnson, "Impact of loading-dependent intrinsic framework flexibility on adsorption in UiO-66," *J. Phys. Chem. C* **126**(41), 17699–17711 (2022).